Loss of GFAP cause retinal dysplasia and vision impairment

Menachem Viktor Khamo Sarusie [1,2], Cecilia Rönnbäck [3], Cathrine Jespersgaard [1], Yeasmeen Ali [4], Søren Tvorup Christensen [4], Karen Brøndum-Nielsen [1], Kjeld Møllgård [2], Thomas Rosenberg [3], Lars Allan Larsen [2]*, and Karen Grønskov [1]*.

[1] Kennedy Center, Department of Clinical Genetics, Rigshospitalet, University of Copenhagen, 2600 Glostrup, Denmark. [2] Department of Cellular and Molecular Medicine, University of Copenhagen, Copenhagen, Denmark. [3] Department of Ophthalmology, Rigshospitalet-Glostrup, University of Copenhagen, 2600 Glostrup, Denmark. [4] Department of Biology, University of Copenhagen, Copenhagen, Denmark.

* Corresponding authors:
Karen Grønskov, Kennedy Center, Department of Clinical Genetics, Rigshospitalet, University of Copenhagen, 2600 Glostrup, Denmark., e-mail: Karen.Groenskov@regionh.dk. Lars Allan Larsen, Department of Cellular and Molecular Medicine, University of Copenhagen, Blegdamsvej 3, DK-2200 Copenhagen, Denmark, e-mail: larsal@sund.ku.dk

Keywords: GFAP, Retinal dystrophy, Alexander's disease.

ABSTRACT

Alexander Disease is a rare leukodystrophy caused by gain-of-function variants in the gene encoding Glial Fibrillary Acidic Protein (GFAP), a major constituent of the intermediate filament of Astrocytes within the central nervous system. Currently, no phenotypic consequence of GFAP haploinsufficiency is known, and recent rodent experiments suggest that antisense oligonucleotide-mediated suppression of GFAP expression can reverse the disease progression in AxD.

We investigated a six-generation family with ten individuals presenting with visual impairment, retinal dysplasia and pseudopapilledema. Whole genome sequencing of three affected individuals revealed a rare novel loss-of-function variant in GFAP, which segregated with disease in the family. The variant, c.928dup, results in frameshift and translation into a 422 aa protein (p.Met310Asnfs*113) wild type GFAP is 431-438 aa). Analysis of human embryonic tissues showed strong GFAP expression in retinal neural progenitors in the developing eye at 35-51 days post conception. Experiments using zebrafish models verified that the c.928dup variant does not result in extensive GFAP protein aggregation. Analysis of zebrafish loss-of-function gfap mutants, showed that depletion of GFAP causes vision impairment and retinal dysplasia, characterized by a significant loss of Müller glia cells and photoreceptor cells. Our findings provide novel insight into the function of GFAP and the consequence of GFAP deficiency.

Introduction

Glial Fibrillary Acidic Protein (GFAP) is an intermediate filament protein, expressed in astrocytes of the adult central nervous system (CNS) and retina of mammal[1,2]. In the developing human brain, GFAP is expressed in radial glial cells (RGCs) from 6 weeks post conception (wpc) and in astrocytes from 14 wpc[3]. The expression of GFAP in the developing retina is less well studied. Early immunohistochemical analyses did not reveal GFAP expression in retinal tissue of mouse embryos (E12-E20) [4], while a more recent study, based on embryos obtained from *S. canicula* (small-spotted catshark), identified GFAP expression in retinal progenitors at early developmental stages and in Müller glia cells at later stages[5].

Rare variants within the *GFAP* gene cause Alexander disease (AxD, OMIM #203450) - a rare autosomal dominant inherited severe leukodystrophy, with variable onset ranging from infant to adult life[6]. AxD is characterized by Rosenthal fibers (RFs), which are dense inclusions within astrocytes of the forebrain and/or hindbrain, caused by aggregation and accumulation of GFAP[7,8]. The majority of *GFAP* variants identified in AxD patients are de novo heterozygous missense variants, while a few cases with variants leading to in-frame protein alterations have been reported[8]. A single patient, carrying a *GFAP* nonsense variant (p.E312*), with a mild form of AxD has been reported[9]. The apparent absence of loss-of-function *GFAP* variants in patients, combined with supporting evidence from mouse models, suggest that AxD is caused by GFAP toxicity through a gain-of-function mechanism[7,10]. Recent research in rodent models of AxD proposes that suppression of GFAP expression, through *Gfap*-targeted antisense oligonucleotides, is a promising therapeutic approach to reverse the disease progression in AxD[11,12]. With these exiting and encouraging results in mind, it is important to delineate the normal function of GFAP and any possible side effects from suppression of GFAP.

Here, we report the investigation of a large Danish family segregating a rare form of optico-retinal disorder, characterized by pseudopapilledema and poorly defined inner retinal layers. Clinical heterogeneity was observed. Genetic analysis led to identification of a novel loss-of-function variant of GFAP segregating with the disease in the family. Functional studies in zebrafish *gfap*$^{-/-}$ mutants confirmed that GFAP plays an important role in retinal development and that loss of GFAP may cause visual impairment.

Results

Identification of a family with inherited retinal dysplasia and pseudopapilledema. A six-generation Danish family with poor vision was discovered and followed during a period of 35 years (Fig. 1a). Clinical examination was performed in four affected family members (IV-6, V-1, V-3 and V-7) with best corrected visual acuity (BCVA) from normal to low vision. The earliest examinations of family members were carried out at age six and seven years. The condition was stationary in individuals followed through decades. Clinical data are presented in Table 1.

The fundoscopic phenotype showed a condition with a dome-shaped pellucid structure covering the optic disc and extending epiretinally and temporally into the papillo-macular area including an atrophy of the foveal pigment epithelium (Fig. 1b, Table 1). Milder expressions were confined to pseudopapilledema with varying degrees of epipapillary glial tissue, blurring of the disc margins, and normal or slightly subnormal visual acuity. No pigmented mass nor retinal dragging was observed in any of the affected individuals. The main arterioles appeared sheeted with a white cuffing from the optic disc and peripherally along the vascular arcades. Individuals V-3 and V-7 with macular atrophy had central scotomas as measured with Goldmann perimetry. Colour vison and dark and light adapted full-field ERG was normal in two affected individuals (Fig.1, V-3 and V-7).

OCT confirmed the abnormal morphology of the optic disc without sign of drusen in individuals V-3 and V-7 (Fig. 1b). The epiretinal glial mass extended temporally to the macular region and the retina showed disorganized inner retinal layering. (Fig. 1b). The tissue complex measured as much as 1.3 mm in height in the subject with the most excessive glial growth. In the fovea of the two subjects (V-3 and V-7) the retina was disorganized and atrophic (Fig. 1b). The latter finding probably explains the poor vision. The retinal picture was symmetrical in the two eyes of all examined individuals.

Fluorescein angiography of individual V-7 showed that the epipapillary glial mass was richly vascularized with small arterioles and capillaries, which continued into the papillomacular area following the nerve fibre pattern. Early and late profuse capillary leakage was present in the posterior pole and at the margins of the central atrophy. All the examined individuals were in good health without signs of any systemic disease.

Identification of a rare variant in the *GFAP* gene. Whole genome sequencing (WGS) with subsequent filtering of variants showed that three affected individuals (V-1, V-3 and V-7) were all heterozygous for five rare coding variants, which were not present in an unaffected individual (VI-3) (Fig. 1a). Two of the five variants were synonymous (*PEMT* p.Pro19= and *OR10H2* p.Thr116=), not predicted to affect splicing using the spice predictors in Alamut Visual, and were not further analysed. Two variants were missense variants (*GAS2L2* p.Pro288Leu and *SOST* p.Ala28Val). Biallelic variants in *GAS2L2* are associated with primary ciliary dyskinesia (OMIM 618449)[13]; furthermore, ACMG classification of the variant is VUS (variant of unknown significance). Monoallelic variants in *SOST* are associated with Craniodiaphyseal dysplasia (OMIM 122860)[14] and biallelic variants are associated with Sclerosteosis 1 (OMIM 269500)[15]. According to ACMG guidelines, the variant is classified as VUS, but the presence of 19 alleles out of 251433 in gnomAD v2.1.1 database, would be considered too high for a severe dominant disease with onset in childhood. We therefore considered it unlikely that these four variants were the cause of retinal dysplasia in the family.

Analysis of additional family members IV-4, IV-6, V-8 and VI-4 showed that the variant in *GFAP* segregated with the retinal dysplasia phenotype in the family, however one case of non-penetrance was observed (individual IV-6). The variant NC_000017.11:g.44911435dup (NM_002055.5:c.928dup) within the coding region of *glial fibrillary acidic protein* (*GFAP*) gene is predicted to result in a frameshift at codon 310, and termination after incorporation of 112 aberrant amino acids (p.Met310Asnfs*113). The variant is not present in the 125,748 exomes and 76,156 genomes of Genome Aggregation Database (gnomAD v.2.1.1) and it is classified as "likely pathogenic" according to ACMG guidelines (PVS1_moderat, PM2_supportive, PP1_strong).

Expression of GFAP in retinal neural progenitors of the developing human eye.

To investigate the expression pattern of GFAP in the developing human retina, we performed immunohistochemical analysis of human embryonic and fetal tissue sections at different stages of eye development. We observed strong expression of GFAP in retinal neural progenitors (RNPs) as early as 35 days post conception, dpc (Fig. 2a-b). At 51 dpc we observed strong GFAP expression in early RNPs near the ciliary body and gradually weaker expression in more differentiated RNPs in regions closer to the optic nerve papilla (Fig. 2c). Immunostaining of a 13 weeks post conception eye showed very weak GFAP expression in Müller Glia Cells, but strong expression in astrocytes, entering the retina from the optic nerve (Fig. 2d-f).

The c.928dup mutation does not result in extensive GFAP protein aggregation.

A hallmark of AxD pathology is the presence of Rosenthal fibers, which are cytoplasmic protein aggregates in astrocytes of the brain, predominantly formed due to missense mutations in *GFAP*[7,8]. We first assessed the protein aggregation properties of the p.Met310Asnfs*113 GFAP variant *in vivo*, by expressing the variant N-terminally fused to GFP under a zebrafish *gfap* promoter and quantified the number of aggregates as previously described[16]. For comparison, we repeated the experiment with full-length WT and a known AxD missense GFAP variant (p.R79C). As expected, the p.R79C GFAP variant resulted in extensive protein aggregation in the spinal cord and brain compared to the WT GFAP variant (Fig. 3a, 3a'). In contrast, we found that there was no significant difference in the number of aggregates between WT and c.928dup GFAP variant (Fig. 3a, 3a'). Western blot (WB) analysis showed that the p.Met310Asnfs*113 variant protein was present at its full-length form indicating that the absence of GFAP aggregates was not due to protein degradation *in vivo* (Fig. 3b). This suggest that the disorder observed in proband patients with the c.928dup *GFAP* allele have a different pathological mechanism than that seen in AxD patients.

Loss of function mutation in the zebrafish *gfap* gene cause retinal dysplasia. Given that the c.928dup *GFAP* variant causes an extensive out-of-frame amino acid incorporation, we hypothesized that a disruption in protein function causes the clinical outcome observed in ORED patients. To investigate whether *GFAP* loss of function disrupts eye development *in vivo*, we next used the CRISPR/Cas9 system to induce deletions in the zebrafish *gfap* promoter and exon 1, in order to silence expression and diminish potential genetic compensation[17]. We identified and characterised two phenotypically similar alleles with a 460 bp (*gfapΔ460*) and 561 bp deletion (*gfapΔ561/ins21*), respectively, spanning the TATA-box among other elements in the *gfap* promoter region as well as the start-codon in the first exon. These *gfap* promoter-less mutants displayed an expected reduction in *gfap* mRNA and protein expression levels (Supplementary Fig. S1).

Gross assessment of the promoter-less mutant progenies ($gfap^{+/-}$ and $gfap^{-/-}$), revealed a phenotype resembling the atrophic retina observed in our patients, however more severe affecting the development of the whole eye. At two days post fertilization (dpf) gfap+/- and gfap-/- larval eye diameter was indistinguishable from WT siblings (Fig. 4a, a'). At 6 dpf we observed a mild but significant decrease in eye diameter without other gross abnormalities (Fig. 4a''). To test the specificity of the eye developmental phenotype in the *gfap* promoter-less

mutants, we performed rescue experiments by injection of WT and mutant *human GFAP* mRNA into the progeny from *gfap*$^{+/-}$ in-cross zebrafish and correlated eye diameter measurements to each genotype group. We found that WT *GFAP* mRNA, but not mRNA encoding p.Met310Asnfs*113 protein rescued the eye diameter phenotype in *gfap*$^{+/-}$ and *gfap*$^{-/-}$ mutants (Fig. 4b, b'). Transverse sections of the eyes and brain of the *gfap* mutant larvae showed normal formation of retinal layers at 2, 4 and 6 dpf, however at 6 dpf the number of cells in the ganglion cell layer (GCL) was decreased significantly in sections around the optic nerve (Fig. 5a, b). In seven months post fertilization (mpf) adult fish the retina was smaller in *gfap* mutant fish due to thinner GCL, INL and ONL (Fig. 5c). Reduction in eye size during retinal development is likely attributed to an increment in apoptosis detected in the inner layers of the eye (including the lens) as early as 52 hours post fertilization (hpf) (Fig. 5d, d').

Since the eye size changes may correlate with vision impairment, we determined the startle response to sudden changes in the light conditions and optomotor response (OMR) for wildtype siblings and *gfap*$^{+/-}$ and *gfap*$^{-/-}$. The startle response protocol consisted of six dark to light switches (Fig. 6a). During the testing period the distance travelled by *gfap*$^{+/-}$ and *gfap*$^{-/-}$ larvae during light period was less than their WT siblings (Fig. 6a') and exhibited an average increase of 44 % and 46 % in the proportion of larvae that were unresponsive to repeated off/on light cycles compared to their WT siblings (Fig. 6a'). We observed similar indication of vision impairment when assessing the OMR of *gfap*$^{+/-}$ and *gfap*$^{-/-}$ larvae which showed increased inactivity and decreased duration spend swimming at high velocities when compared to WT siblings (Fig. 6b, b').

GFAP is expressed in retinal progenitors of the vertebrate developing eye[5]. The expression of GFAP is known to be highly upregulated in retinal Müller glial cells (MGC) in response to retinopathies, thus suggesting that MGCs share properties with retinal progenitors. To determine whether MGC were affected by loss of GFAP function during early eye development we labelled MGC with the radial glia and astrocyte marker BLBP[18]. At 6 dpf and in 7 mpf adult fish we observed a visible reduction in the number of BLBP^{+} MGCs in the INL in the *gfap*$^{+/-}$ and *gfap*$^{-/-}$ mutants compared to their WT siblings, which was not the case at earlier stages (Fig. 7a). As indicated by the BLBP marker expression in 6 dpf *gfap*$^{+/-}$ and *gfap*$^{-/-}$ mutants, the MGCs that remained in the ONL had reduced cell body area, thinning of processes and visibly fewer apical branches at the base of rods and cones in the ONL suggesting that these MGCs were dysfunctional (Fig. 7a, a').

MGCs are responsible for generation and maintenance of neuronal, rod and cone lineages in the eye during fish postembryonic development and retinal homeostasis in the mammalian eye [19,20]. Given the observed MGC pathology in *gfap*$^{+/-}$ and *gfap*$^{-/-}$ mutants, we examined rod and cone development during early postembryonic development and adult eye. At four and six dpf, we observed a mild and significant decreased number of ZPR3^{+} outer segments rods and double cone cells in the ONL of *gfap* mutants, respectively (Fig. 7b, b'). The retained nuclear signal in weak ZPR3^{+} cells suggest delayed photoreceptor cell differentiation during early postembryonic development. Similarly, in 7 mpf adult fish *gfap*$^{+/-}$ and *gfap*$^{-/-}$ retina we observed loss of ZPR3^{+} rods (Fig. 7b, b') and tearing in the tissue (Fig. 7b), albeit with different penetrance. In order to determine the extent of ZPR3^{+} photoreceptor loss at the pituitary macular region in our *gfap* mutants, we performed 3D reconstruction whole juvenile (14 dpf) and adult eyes (9 mpf). When comparing WT siblings with *gfap*$^{+/-}$ at juvenile stage, photoreceptor cells at the pituitary macular region in the mutant were more affected than those around the optic nerve and periphery regions (Fig. 7c). In contrast, ZPR3^{+} photoreceptor cell loss was observed in the periphery regions in adult *gfap*$^{+/-}$ and *gfap*$^{-/-}$ eyes as well as the pituitary macular region with *gfap*$^{-/-}$ being more affected than *gfap*$^{+/-}$ (Fig. 7c).

DISCUSSION

Zebrafish GFAP mutants recapitulates key retinal abnormalities found in affected individuals

In our study we examined a family with members with reduced visual acuity carrying a novel nonsense mutation in *GFAP* (c.928dup; p.Met310Asnfs*113) that partially delete the 2B rod domain and result in a frameshift of 112 amino acids. Our clinical examination of the affected individuals in the family revealed retinal defects with varied severity that could be identified as early as six years of age. The observed retinal dysplasia was stationary across decades in the examined individuals and some individuals reported mild difficulties in swallowing, but otherwise in good health. It should be noted that AxD is a heterogeneous disease that can result in mild or even asymptomatic cases despite remarkable atrophy of the brainstem and spinal cord on MRI[21]. In fact, a nonsense mutation variant in proximity of our variant has been reported to cause a relative mild AxD case (c.1000 G>T, p.E312*)[9]. Previous studies, could indicate that the p.Met310Asnfs*113 variant we identified in the family, would form aggregate as overexpression of GFAP without the tail domain result in formation of polymorphic

aggregates[22,23]. However, given the large number of out-of-frame amino acid incorporated the outcome is unpredictable and GFAP aggregation and AxD outcome is complicated further by the expression of different GFAP isoforms and mis-splicing in humans, which are difficult to model in animals[24,25]. Lastly, at present we cannot rule out that the c.928dup *GFAP* variant produces transcripts that undergo nonsense-mediated-decay in the affected individuals[26]. Taken together, we cannot completely exclude a possibility that the affected individuals represents asymptomatic cases of AxD. However, the stationary nature of the clinical signs and given that our *in vivo* aggregation assay did not show extensive GFAP aggregation upon overexpression of the p.Met310Asnfs*113 variant, we find this scenario unlikely. Operating on the presumption that a gain-of-function is unlikely, we generated a promoter-less GFAP mutant in zebrafish. This was based on that previous attempts to generate a GFAP null animal have used classic gene knockout methods, which raised the possibility of genetic compensation. In fact, several studies of *Gfap* null mice reported normal development, growth, fertility and lifespan[27–31]. Although obvious candidates for compensation (such as vimentin and nestin) were ruled out[28,32,33] , recent studies in vertebrates have proven genetic compensation to be more complex, involving mutant mRNA degradation resulting in upregulation of genes that exhibit sequence similarity to mutant gene mRNA[17,34].

Characterisation of our zebrafish promoter-less GFAP mutants demonstrated increased apoptosis in the eye during late embryonic retinal development and phenotypically smaller eyes with visual impairment at later larvae stages. Although the small eye phenotype was not directly observed in the affected individuals, it likely occurred due to a combination of several phenotypes observed. Fewer cells in the GCL, ONL and cell shrinkage are factors which may influence neurogenesis, intraocular expansion and cellular hypertrophy determine retina size in the larvae and adult fish[35]. The small eye phenotype in the mutants appeared to be specific for GFAP function, as demonstrated by rescue experiments with c.928dup mRNA. In addition, heterozygous mutants also suggested that the p.Met310Asnfs*113 variant was partially functional. Given the early expression of GFAP in immature and mature MGCs in the INL, the phenotypes are likely caused by abnormal MGC function. Indeed, at the symptomatic larvae stages of the mutants we observed fewer MGCs in the INL and those remaining displayed smaller soma with abnormal processes and branching at the ONL as a consequence of weaker BLBP expression. In the brain, *Blbp* transcription is induced in radial glia by migrating neurons through Notch signalling and blocking BLBP function radial glia decrease the number of radial processes extended[18,36]. Concurrently with abnormal BLBP marker expression in MGCs, we

observed initial delayed photoreceptor maturation in the retina, which appeared to progress to photoreceptor cell loss and tearing of the retina as the fish aged. This finding is in agreement with evidence for a lineage relationship between the proliferative MGCs and the rod precursors. MGC function to serve as a scaffold upon which rod progenitors migrate from the INL to the ONL and provide tensile strength to the developing retina. The latter may in part explain changes in the cell number found in the GCL of larvae fish as well as layer thickness changes in adult mutant fish [20,37–41]. The progressive nature of the condition is unlike the case in our affected individuals in which the dysplasia and macular degeneration was stationary. A probable explanation for this is that the retinas of postembryonic teleost fish develop faster and continue to grow for their lifetime, while the human retina stops developing around 20 years of age[42].

MGCs and GFAP has a role during early embryonic retinal development

A common perception is that MGCs cannot facilitate or organize differentiation of the other retinal cell type as MGCs themselves are not present during retinal development. This has been strengthened by early 3H-thymidine birth-dating studies in rodents demonstrating that Müller glia are among the last retinal cells to be produced from retinal precursors[43,44] . A chronological order for retinal development has also been supported by a recent comprehensive transcriptomic study of human retinal samples from 4 to 19 wpc[45]. However, anatomical evidence suggests that cells with some properties of MGCs are present at early stages in retinal development[46]. The anatomical studies suggest that Müller glia undergo a gradual maturation from neuroepithelial cells (perhaps with some properties of radial glia) to mature Müller glia, and thus are present in an immature form at the onset of retinal differentiation[46,47]. The presence in the early developing retina of cells with the properties of Müller glia has been supported by several studies using techniques such as scanning electron microscopy analysis[48,49] and morphological analysis by Golgi-staining[50].

In our study we focused on GFAP expression in early human retinal development. Although GFAP is expressed by MGCs and astrocytes in the retina of all vertebrates the timing and condition varies among species. In mice, GFAP expression appear to be only detected in astrocytes at the optic nerve but not in MGCs during embryonic retinal development and postnatal development[4,51–53]. Robust GFAP expression in MGCs however occurs during reactive gliosis, in response to injury or disease in rodents[53] and fish[54,55]. Previous studies

indicated that GFAP is expressed during human fetal retina development from 8 wpc, but like in mice its expression was observed only in astrocyte precursors that had migrated to the optic nerve head[56,57]. GFAP expression intensifies following astrocyte precursor maturation and migration into the vascularized central retina beginning around 16-18 wpc[57,58]. In contrast, our findings suggest that robust GFAP expression occur in retinal progenitor cells (RPCs) throughout the neural retina (NR) of the human developing fetal eye already at 35 dpc. By 51 dpc we observed strong expression in RPCs in the region near the ciliary body and weaker expression in differentiating RPCs in the retina region near the optic nerve papilla. At thirteen wpc, some of these RPCs mature into MGCs resulting in significant downregulation of GFAP expression with expression retained at distal processes and end-feet. Our observed appearance of mature MGCs is in agreement with a recent report dating it to 12 wpc[45], while in another study determined the timing to be 18-19 wpc[58]. The late MGC appearance in the latter study likely reflects the use of CRALBP as MGC marker, which is expressed late during their function in the retinal visual cycle[59]. GFAP expression in human RPCs have not previously been observed, but our observations remarkably resemble the GFAP immunoreactivity pattern during embryonic retinal development in catshark fish and zebrafish. In catshark fish, GFAP expression occur in the pre-neurogenic retina of catshark (*S. canicula*) in NECs, which during the neurogenic developmental stage elongate and transform into RGCs to an asymmetric mode of cell division that coincides with the beginning of neurogenesis[5]. Similarly, transgenic studies in zebrafish demonstrate that GFAP expression occur prior to histological differentiation of the retina primordium at 24 hpf with mitotically active MGCs first appearing around 48 hpf [19,60]. Examination of MGC origin during zebrafish eye development have demonstrated at least two distinct steps in MGC maturation[47]. Together our observations indicate that GFAP expressing precursors to MGCs exist during early human retinogenesis, which resemble fish embryonic retinal development.

In conclusion, our data show that GFAP plays an important role in retinal development and that loss of GFAP can cause retinal dysplasia and vision impairment.

MATERIAL AND METHODS

Family pedigree and clinical investigations

The pedigree encompassed six generations followed for 35 years. All available patient files were retrieved and scrutinized and a re-investigation of five affected, one unaffected, and one

non-penetrant individual was made. Re-examinations took place at the Department of Ophthalmology, Rigshospitalet, Copenhagen.

Standard ophthalmological examination was performed in all seven individuals including best corrected visual acuity (BCVA) according to the ETDRS procedure. The subjects underwent fundus photography (Topcon), spectral-domain-optic coherence tomography (SD-OCT) (Heidelberg Eye Explorer) including autofluorescence photography, one of the subjects had fluorescence angiography, indocyanine green angiography, adaptive optics, and full-field ERG.

Written informed consent was obtained from all participants. The study was approved by the National Committee on Health Research Ethics, Denmark (journal number 1301394) and followed the tenets of the Declaration of Helsinki.

Molecular genetic analysis

Blood samples were obtained for eight family members (IV-4, IV-6, V-1, V-3, V-7, V-8, VI-3, VI-4) and high molecular DNA was extracted using the Chemagic 360 machine (Perkin Elmer, Waltham, Massachusetts, USA). Whole genome sequencing was performed by BGI Group (Shenzhen, China) using Illumina HiSeq X-ten. A mean coverage of 30 X were provided. Alignment was performed to NCBI hg19 version of the human genome using BWA software. GATK (Broad Institute, MIT Harvard, Cambridge, MA, USA) was used for variant calling (SNV and indels). Three affected (V-1, V-3, V-7) and one unaffected (VI-3) individual were analyzed. A total of 398,394 unique variants were retrieved for the four samples. The VarSeq program (Golden Helix, Bozeman, Montana, USA) was used for filtering. Coding variants (including 8 bp flanking intron sequence) with a minor allele frequency (MAF) below 0.5% in the gnomAD v2.1.1 database (https://gnomad.broadinstitute.org/) and an allelic frequency between 0.3 and 0.7 were retrieved. The zygosity of affected individuals were set to heterozygous whereas the unaffected individual was set to reference. The Alamut Visual Plus program (Lausanne, Switzerland and Boston, Massachusetts, USA) were used for further analysis of variants.

Segregation analysis was performed using primers GFAP-ex6-FH acccactgcttactggcttatcGAGATGCCAGGGGAGAAGG and GFAP-ex6-RH gaggggcaaacaacagatggcCAGGGCCAGCTTGACATTG for PCR amplification and

subsequent Sanger sequencing. Capital letters are gene specific and small letters are used for subsequent sequencing. Sequencing was performed using BigDye v3.2 terminators (Applied Biosystems, Waltham, Massachusetts, USA) and analysis on an ABI3130XL (Applied Biosystems).

Immunohistochemistry of human embryonic and fetal eyes

Four human embryos and 5 fetuses were obtained from legal abortions after informed consent from all contributing women following oral and written information, in accordance with the Helsinki Declaration II, and was approved by the Danish Regional Committee on Health Research Ethics (KF–V.100.1735/90) & (KF-11 2006 – 4838).

Immediately following the abortion, entire embryos of 35 dpc, 51 dpc and 53 dpc (days post conception) and fetal eyes from fetuses of 13, 15 and 19 wpc (weeks post conception) were removed and promptly fixed for 12–24 h at 4 °C in either 10% neutral buffered formalin, 4% formol-calcium, Lillie's or Bouin's fixatives. This procedure kept the time from delivery to fixation at a minimum, normally less than 2 h, in order to retain optimal tissue quality. Prior to paraffin embedding, the specimens were dehydrated with graded alcohols, and cleared in xylene. Then 3 - 6 μm thick serial sections were cut in transverse, sagittal or horizontal planes, and placed on silanized glass slides.

Sections were deparaffinized and rehydrated in xylene following standard protocols. Endogenous peroxidase was quenched using a 0.5% solution of hydrogen peroxide in TBS for 15 minutes. Following rinses with TRIS buffered saline (TBS, 5 mM Tris-HCl, 146 mM NaCl, pH 7.6), non-specific binding was inhibited by incubation for 30 minutes with 10% goat serum at room temperature. The sections were incubated overnight at 4oC with primary antibodies (Table 1) diluted in blocking buffer and washed with TBS. For bright field light microscopy analysis, the REAL EnVision Detection System (Peroxidase/DAB+ rabbit/mouse, code K5007, DakoCytomation, Glostrup, Denmark) was used for detecting mouse and rabbit primary antibodies. The sections were washed with TBS. Positive staining was recognized as a brown color. The sections were counterstained with toluidine blue or Mayers hematoxylin and dehydrated in graded alcohols and coverslipped with Pertex mounting media.

Details of the primary antibodies including dilutions and suppliers are listed in Supplementary Table S2. Control sections were incubated with mouse IgG1 or irrelevant rabbit antibodies, as well as subjected to omission of primary or secondary antibodies. These were always blank.

Zebrafish husbandry

The AB Wild-type (WT) zebrafish strain was obtained from the Zebrafish International Resource Center and maintained in the animal facility of the University of Copenhagen. The WT were raised at 28°C and kept in a constant LD cycle according to standard protocols. All experiments and animal handling procedures were approved and conducted under licenses from the Danish Animal Experiments Inspectorate (Protocol code: P18-120/P20-387). Staging of zebrafish in hpf was carried out as previously described (Kimmel et al., 1995).

Generation of promoter-less gfap mutants

The promoter motifs of the zebrafish *gfap* promoter were mapped using the Eukaryotic promoter database (https://epd.epfl.ch/). Based on the location of the motifs, crRNAs were designed and evaluated using the IDT CRISPR design (Integrated DNA Technologies), CCTop and CRISPOR tools. A pair of crRNAs was selected with a target region upstream of the 5' UTR (IDT Design ID: CD.Cas9.JPYK4256.AC) and downstream of the *gfap* start-codon, respectively (IDT Design ID: Dr.Cas9.GFAP.1.AL). The CRISPR-Cas9 RNP complex was assembled according to the manufacturer's protocol for zebrafish embryo microinjections. Briefly, equimolar amounts of crRNAs and tracrRNA were mixed in a nuclease-free duplex buffer to create a 3 µM gRNA complex solution. The gRNA solution complex was mixed with an equal volume of 0.5 µg/µL HiFi Cas9 Nuclease V3 (IDT) protein solution diluted in Cas9 working buffer (20 mM HEPES-KOH, 150 mM KCl, pH 7.5). The gRNA/Cas9 mixture was incubated at 37°C for 10 min to assemble the RNP complex and 1 nl was microinjected into the cytoplasm of each one-cell staged embryos.

Eye with measurements

Measurements of the left and right eye width were conducted blindly from Z-series of mRNA injected (100 pg) and uninjected hetereozygous incrosses from different pairs at 2 and 6 dpf. The Z-series were collected with a Zeiss Axio Zoom.V16 microscope equipped with a AxioCam 705 color camera (Interval thickness: 5.0 µm) from individual larvae anesthetized in

0.02% tricaine methanesulfonate (Sigma-Aldrich, A5040) and mounted in 3 % methylcellulose.

Total RNA isolation and qRT-PCR

To determine the degree of endogenous *gfap* promoter silencing in the promoter-less mutants, RNA was extracted from a pool of homozygous outcrosses, and in-crosses of wildtype sibling and homozygous from three different pairs using the RNA isolation kit (Zymo Research). One microgam of total RNA was reverse transcribed using SuperScript™ II (Invitrogen, Carlsbad, CA), and oligo-dT primers (Invitrogen). To detect gfap cDNA (NM_131373.2), qRT-PCR was performed using Brilliant III Ultra-Fast SYBR® Green QPCR master mix (Agilent Technologies) with the primers 5′-GGATGCAGCCAATCGTAAT-3′ (forward) and 5′-TTCCAGGTCACAGGTCAG-3′ (reverse). The qRT-PCR reactions were performed in triplicate and were analyzed on an ABI 7500 fast system. The data was normalized against the average expression value of the housekeeping gene b-actin2.

Cloning of GFAP fusion and transcription of mRNA from full-length constructs

The GFAP p.(Met310Asnfs*113) fusion construct was cloned by site-directed mutagenesis of the mini-Tol2 vector containing the human WT GFAP construct[16] introducing the nucleotide duplication at position 928. Subsequently another round of site-directed mutagenesis was performed to remove the stop-codon generated by the frameshift and the remaining ORF. For mRNA generation the GFAP cDNA was amplified from a universal human cDNA library (Takara Bio) and subcloned into the pCS2+ vector using the XhoI/SnaBI sites. The c.928dup mutation was introduced by site-directed mutagenesis with the full-length vector as previously described for the fusion construct. Capped mRNA was generated *in vitro* after NotI linearization with the mMESSAGE mMACHINE Kit (ThermoFisher) kit and purified according to manufactures instructions. All plasmids were verified by DNA sequencing (ABI3130xl Genetic Analysers). Primers used for PCR and cloning are listed in Table S1.

GFAP aggregation assay

The GFAP aggregation assay was performed as previously described[16]. Briefly, expression vectors containing the WT, p.Arg79Cys and p.(Met310Asnfs*113) GFAP construct were microinjected into the cytoplasm of One-cell stage zebrafish embryos (50 pg). At 30 hpf the embryos were anesthetized and mounted in 3% methylcellulose for imagining. Z-series of the head and trunk regions were collected (Interval thickness: 4.0 µm) with a Zeiss Axio Zoom.V16

microscope equipped with a AxioCam 705 color camera. GFAP aggregates were blindly counted using the Cell Counter plugin in ImageJ (Fiji). Representative stacking images were assembled in ZEN 3.2 Pro (Zeiss) and Photoshop CS6 software (Adobe).

Western Blot

Prior to protein extraction, microinjected larvae (30 hpf) were manually dechorinated, anesthetized and deyolked in Deyolking buffer (55mM NaCl, 1.8mM KCl, 1.25mM $NaHCO_3$) at 1100 rpm. Deyolked larvae were collected at 3000rpm, 4ºC and rinsed several times in Wash buffer (110mM NaCl, 3.5mM KCl, 10mM Tris pH 8.5, 2.7mM $CaCl_2$). The larvae were subsequently lysed in Protein extraction buffer (1% SDS and 10mM Tris pH 7.4) with proteinase inhibitors and flash-freezed. Western blot was carried out as previously described in Schrøder et al., 2011 using horseradish peroxidase-conjugated secondary antibodies. Blots were developed with FUSION-Fx chemiluminescence system (Vilber Lourmat) while images were processed and analysed in Photoshop CS6 and ImageJ (Fiji), respectively. Primary antibodies for western blot and immunofluorescence are listed in Table S2.

Sectioning, H&E and immunofluorescence

For sectioning, 2, 4 and 6 dpf zebrafish larvae from heterozygous in-crosses were collected and fixed in 4% paraformaldehyde (PFA) overnight at 4 °C. Larvae were rinsed in PBS, genotyped and their heads embedded and orientated in 5% agarose. Genotyped adult fish were fixed in 4% PFA for several days at 4ºC after anesthetizing and euthanizing the fish. The eyes were carefully enucleated, embedded and orientated in 5% agarose. The agarose blocks were dehydrated in increasing alcohol solutions over several days (70%/96%/99% EtOH). Following dehydration of the agarose block, the block was transferred into Xylene and into paraffin overnight at 60 °C. The block was embedded into fresh paraffin prior to sectioning and slide collection (Thickness: 5 µm). Slides with the sections were dried overnight at 37 °C followed by standard haematoxylin and eosin staining or immunofluorescence. Haematoxylin and eosin-stained slides were imaged on AxioScan 7 slide scanner (Zeiss) and immunofluorescence-stained slides were imaged on LSM710 confocal system (Zeiss).

TUNEL assay

For the TUNEL assay, embryos were fixed in 4% paraformaldehyde for 2 hours at room temperature and kept in 100% methanol overnight at -20ºC. After gradual rehydration and genotyping, apoptotic cells were detected using the ApopTag peroxidase in situ apoptosis

detection kit (Millipore). The samples were mounted in glycerol and Z-series of the right eye was collected (interval thickness: 3.0 µm) with Axio Zoom.V16 microscope equipped with a AxioCam 705 color camera (Zeiss).

ECi-DEEP-Clear of the zebrafish eye

The clearing protocol for the eye was adapted from the DEEP-Clear protocol[61]. Unless otherwise stated the pH for solutions were neutral (pH 7-7.4). Zebrafish samples were first anesthetized with 0.04% tricaine methanesulfonate (Sigma-Aldrich, A5040) and euthanized. This was followed by immediate fixation in 4% paraformaldehyde at 4°C for 1-3 days and removal of fixative by rinsing in PBS several times at room temperature. For adult fish, eyes were carefully enucleated and dehydrated in pre-chilled acetone overnight at -20°C. After acetone treatment, samples were pre-treated with 3% H_2O_2 in Acetone for 30min at room temperature and gradually rehydrated in 75%, 50% and 0% acetone in PBS. Guanine crystals in the eye were dissolved by long rinses in PBS pH 6.0[62]. After several short dH_2O rinses, samples were first depigmented by bleaching in 3% H_2O_2/1% KOH for approx. 45 min to 4 hours under strong light, followed by hydrophilic depigmentation in 8% THEED (Sigma-Aldrich, 87600) and 5% Triton-X in PBS pH 9-10, at 37°C for 30 min to 2 days. Depigmentation durations were dependent on the developmental stage. After several PBS rinses, unspecific antibody binding was blocked in PBDT (1% DMSO, 1% BSA, 0.1% Tween20, 0.5% Triton X-100, 5% goat serum, PBS) and samples incubated with primary antibodies in PBDT overnight at 4°C. Unbounded antibodies were subsequently removed by several PBSTT (0.1% Triton-X, 0.1% Tween20, PBS) rinses at room temperature and incubated with secondary antibodies in PBDT overnight at 4°C. Following another round of PBSTT rinses, the samples were nuclear stained with SYTOX Deep Red Nucleic Acid Stain (Thermo Scientific, S11381) at room temperature and mounted in 2% agarose. Samples were then gradually dehydrated in 20%, 50%, 80% and 99% ethanol in dH_2O pH 9-10 at room temperature and immediately RI matched in ethyl cinnamate (Sigma-Aldrich, 8.00238). Samples were imaged on a Zeiss CellObserver Spinning Disk confocal system or Light Sheet 7 (Zeiss).

Startle response and optomotor response (OMR) assay

Prior to conducting the assay, fed larvae were cultured in a light environment for at least 1 hour. For startle response assessment, 7 dpf larvae were carefully transferred to a 48-well plate with 1 mL E3 medium. The plate was inserted into the Zebrabox (Viewpoint, France) allowing

the fish to readapt to the equipment light conditions before subjected to six Dark-Light cycles ending with a dark period during motion tracking. Dark duration was set to 1 second and Light duration was set to 30 seconds. The overall activity of the fish was recorded in one second-bins for a total duration of 33 minutes and 7 seconds. For OMR, 9 dpf larvae were carefully transferred to a 10 well OMR plate (Viewpoint, France) with E3 medium. Adaptation to a white background (bottom screen) and lighting conditions was done for at least 1 hour inside the Zebrabox (Viewpoint, France). Subsequently the background was changed into moving black horizontal stripes on a white background (10 stripes, 30 rpm, 25 fps) and fish locomotion was recorded for 5 minutes in 5 second bins. Swim speed was recorded in four categories: Fast (>8 mm/s), intermediate (3-8 mm/s) and slow (<3 mm/s) and no activity (no detection of movement). For all experiments "Light" periods were set to 12 % power (Top Light) and "Dark" periods to 0 %, with an infrared illumination and camera recording at 60 frames per second. The detection sensitivity level was set to 21 and minimum size to 3, which focuses the movement detection on the head of each larva and ignores movement of smaller particles.

ACKNOWLEDGEMENTS

We would like to thank Pernille Froh, Ha Nguyen and Pia Skovgaard for expert technical assistance. We acknowledge the Core Facility for Integrated Microscopy, Faculty of Health and Medical Sciences, University of Copenhagen. The study was supported by grants from the Velux Foundation and the Novo Nordisk Foundation.

REFERENCES

1. Messing, A. & Brenner, M. GFAP at 50. *ASN Neuro* **12**, (2020).
2. Tao, C. & Zhang, X. Development of astrocytes in the vertebrate eye. *Dev Dyn* **243**, 1501–10 (2014).
3. Holst, C. B., Brøchner, C. B., Vitting-Seerup, K. & Møllgård, K. Astrogliogenesis in human fetal brain: complex spatiotemporal immunoreactivity patterns of GFAP, S100, AQP4 and YKL-40. *J Anat* **235**, 590–615 (2019).
4. Sarthy, P. V., Fu, M. & Huang, J. *Developmental Expression of the Glial Fibrillary Acidic Protein (GFAP) Gene in the Mouse Retina*. *Cellular and Molecular Neurobiology* vol. 11 (1991).
5. Sánchez-Farías, N. & Candal, E. Identification of radial glia progenitors in the developing and adult retina of sharks. *Front Neuroanat* **10**, (2016).

6. Brenner, M. *et al.* Mutations in GFAP, encoding glial fibrillary acidic protein, are associated with Alexander disease. *Nat Genet* **27**, 117–20 (2001).

7. Hagemann, T. L. Alexander disease: models, mechanisms, and medicine. *Current Opinion in Neurobiology* vol. 72 140–147 Preprint at https://doi.org/10.1016/j.conb.2021.10.002 (2022).

8. Messing, A. Alexander disease. in *Handbook of Clinical Neurology* vol. 148 693–700 (Elsevier B.V., 2018).

9. Nam, T. S. *et al.* Identification of a novel nonsense mutation in the rod domain of GFAP that is associated with Alexander disease. *European Journal of Human Genetics* **23**, 72–78 (2015).

10. Messing, A. Refining the concept of GFAP toxicity in Alexander disease. *Journal of Neurodevelopmental Disorders* vol. 11 Preprint at https://doi.org/10.1186/s11689-019-9290-0 (2019).

11. Hagemann, T. L. *et al.* Antisense suppression of glial fibrillary acidic protein as a treatment for Alexander disease. *Ann Neurol* **83**, 27–39 (2018).

12. Hagemann, T. L. *et al. Antisense therapy in a rat model of Alexander disease reverses GFAP pathology, white matter deficits, and motor impairment*. *Sci. Transl. Med* vol. 13 https://www.science.org (2021).

13. Bustamante-Marin, X. M. *et al.* Lack of GAS2L2 Causes PCD by Impairing Cilia Orientation and Mucociliary Clearance. *Am J Hum Genet* **104**, 229–245 (2019).

14. Kim, S. J. *et al.* Identification of signal peptide domain SOST mutations in autosomal dominant craniodiaphyseal dysplasia. *Hum Genet* **129**, 497–502 (2011).

15. Brunkow, M. E. *et al.* Bone dysplasia sclerosteosis results from loss of the SOST gene product, a novel cystine knot-containing protein. *Am J Hum Genet* **68**, 577–589 (2001).

16. Lee, S. H. *et al.* Aggregation-prone GFAP mutation in Alexander disease validated using a zebrafish model. *BMC Neurol* **17**, (2017).

17. El-Brolosy, M. A. *et al.* Genetic compensation triggered by mutant mRNA degradation. *Nature* **568**, 193–197 (2019).

18. Anthony, T. E., Mason, H. A., Gridley, T., Fishell, G. & Heintz, N. Brain lipid-binding protein is a direct target of Notch signaling in radial glial cells. *Genes Dev* **19**, 1028–1033 (2005).

19. Bernardos, R. L., Barthel, L. K., Meyers, J. R. & Raymond, P. A. Late-stage neuronal progenitors in the retina are radial Müller glia that function as retinal stem cells. *Journal of Neuroscience* **27**, 7028–7040 (2007).

20. Nelson, S. M., Frey, R. A., Wardwell, S. L. & Stenkamp, D. L. The developmental sequence of gene expression within the rod photoreceptor lineage in embryonic zebrafish. *Developmental Dynamics* **237**, 2903–2917 (2008).

21. Sugiyama, A. *et al.* Incidental diagnosis of an asymptomatic adult-onset Alexander disease by brain magnetic resonance imaging for preoperative evaluation. *Journal of the Neurological Sciences* vol. 354 131–132 Preprint at https://doi.org/10.1016/j.jns.2015.05.001 (2015).

22. Quinlan, R. A., Moir, R. D. & Stewart, M. Expression in Escherichia coli of fragments of glial fibrillary acidic protein: characterization, assembly properties and paracrystal formation. *J Cell Sci* **93 (Pt 1)**, 71–83 (1989).

23. Chen, W. J. & Liem, R. K. The endless story of the glial fibrillary acidic protein. *J Cell Sci* **107 (Pt 8)**, 2299–311 (1994).

24. Perng, M.-D. *et al.* Glial fibrillary acidic protein filaments can tolerate the incorporation of assembly-compromised GFAP-delta, but with consequences for filament organization and alphaB-crystallin association. *Mol Biol Cell* **19**, 4521–33 (2008).

25. Flint, D. *et al.* Splice site, frameshift, and chimeric GFAP mutations in Alexander disease. *Hum Mutat* **33**, 1141–1148 (2012).

26. Maquat, L. E. Nonsense-mediated mRNA decay in mammals. *J Cell Sci* **118**, 1773–1776 (2005).

27. Gomi, H. *et al. Mice Devoid of the Glial Fibrillary Acidic Protein Develop Normally and Are Susceptible to Scrapie Prions*. *Neuron* vol. 14 (1995).

28. Mccall, M. A. *et al. Targeted deletion in astrocyte intermediate filament (Gfap) alters neuronal physiology (long-term potentiation/hippocampus/optic nerve/homologous recombination/mouse)*. *Neurobiology* vol. 93 https://www.pnas.org (1996).

29. Pekny, M. *et al.* Mice lacking glial fibrillary acidic protein display astrocytes devoid of intermediate filaments but develop and reproduce normally. *EMBO Journal* **14**, 1590–1598 (1995).

30. Nawashiro, H., Messing, A., Azzam, N. & Brenner, M. Mice lacking GFAP are hypersensitive to traumatic cerebrospinal injury. *Neuroreport* **9**, 1691–6 (1998).

31. Shibuki, K., Gomi, H. & Chen, L. *Deficient Cerebellar Long-Term Depression, Impaired Eyeblink Conditioning, and Normal Motor Coordination in GFAP Mutant Mice*. *Neuron* vol. 16 (1996).

32. Triolo, D. *et al.* Loss of glial fibrillary acidic protein (GFAP) impairs Schwann cell proliferation and delays nerve regeneration after damage. *J Cell Sci* **119**, 3981–3993 (2006).

33. Kamphuis, W. *et al.* GFAP and vimentin deficiency alters gene expression in astrocytes and microglia in wild-type mice and changes the transcriptional response of reactive glia in mouse model for Alzheimer's disease. *Glia* **63**, 1036–1056 (2015).

34. Rossi, A. *et al.* Genetic compensation induced by deleterious mutations but not gene knockdowns. *Nature* **524**, 230–233 (2015).

35. Fernald, R. D. Teleost vision: Seeing while growing. *Journal of Experimental Zoology* **256**, 167–180 (1990).

36. Anton, E. S., Marchionni, M. A., Lee, K. F. & Rakic, P. Role of GGF/neuregulin signaling in interactions between migrating neurons and radial glia in the developing cerebral cortex. *Development* **124**, 3501–10 (1997).

37. MacDonald, R. B. *et al.* Müller glia provide essential tensile strength to the developing retina. *Journal of Cell Biology* **210**, 1075–1083 (2015).

38. Julian, D., Ennis, K. & Korenbrot, J. I. Birth and fate of proliferative cells in the inner nuclear layer of the mature fish retina. *Journal of Comparative Neurology* **394**, 271–282 (1998).

39. Otteson, D. C., D'Costa, A. R. & Hitchcock, P. F. Putative stem cells and the lineage of rod photoreceptors in the mature retina of the goldfish. *Dev Biol* **232**, 62–76 (2001).

40. Mack, A. F., Papanikolaou, D. & Lillo, C. Investigation of the migration path for new rod photoreceptors in the adult cichlid fish retina. *Exp Neurol* **184**, 90–96 (2003).

41. Raymond, P. A., Barthel, L. K. & Curran, G. A. Developmental patterning of rod and cone photoreceptors in embryonic zebrafish. *Journal of Comparative Neurology* **359**, 537–550 (1995).

42. Brown, M. *The Physiology of Fishes*. (1957).

43. Young, R. W. Cell differentiation in the retina of the mouse. *Anat Rec* **212**, 199–205 (1985).

44. Sidman, R. L. Histogenesis of mouse retina studied with Thymidine-H-3. *anatomical record DIV JOHN WILEY & SONS INC, 605 THIRD AVE, NEW YORK, NY* **136**, 10158–0012 (1960).

45. Bulirsch, L. M. *et al.* Spatial and temporal immunoreaction of nestin, CD44, collagen IX and GFAP in human retinal Müller cells in the developing fetal eye. *Exp Eye Res* **217**, (2022).

46. Willbold, E. & Layer, P. G. Müller glia cells and their possible roles during retina differentiation in vivo and in vitro. *Histol Histopathol* **13**, 531–52 (1998).

47. Peterson, R. E., Fadool, J. M., Mcclintock, J. & Linser, P. J. Müller cell differentiation in the zebrafish neural retina: Evidence of distinct early and late stages in cell maturation. *Journal of Comparative Neurology* **429**, 530–540 (2001).

48. Meller, K. & Tetzlaff, W. Scanning electron microscopic studies on the development of the chick retina. *Cell Tissue Res* **170**, 145–59 (1976).

49. Uga, S. & Smelser, G. K. Electron microscopic study of the development of retinal Müllerian cells. *Invest Ophthalmol* **12**, 295–307 (1973).

50. Prada, F. A., Magalhaes, M. M., Coimbra, A. & Genis-Galvez, J. M. Morphological differentiation of the müller cell: Golgi and electron microscopy study in the chick retina. *J Morphol* **201**, 11–22 (1989).

51. Huxlin, K. R., Sefton, A. J. & Furby, J. H. The origin and development of retinal astrocytes in the mouse. *J Neurocytol* **21**, 530–544 (1992).

52. Dorrell, M. I., Aguilar, E. & Friedlander, M. Retinal vascular development is mediated by endothelial filopodia, a preexisting astrocytic template and specific R-cadherin adhesion. *Invest Ophthalmol Vis Sci* **43**, 3500–10 (2002).

53. Bringmann, A. *et al.* Müller cells in the healthy and diseased retina. *Progress in Retinal and Eye Research* vol. 25 397–424 Preprint at https://doi.org/10.1016/j.preteyeres.2006.05.003 (2006).

54. Braisted, J. E., Essman, T. F. & Raymond, P. A. Selective regeneration of photoreceptors in goldfish retina. *Development* **120**, 2409–19 (1994).

55. Wu, D. M. *et al.* Cones regenerate from retinal stem cells sequestered in the inner nuclear layer of adult goldfish retina. *Invest Ophthalmol Vis Sci* **42**, 2115–24 (2001).

56. Božanić, D., Bočina, I. & Saraga-Babić, M. Involvement of cytoskelatal proteins and growth factor receptors during development of the human eye. *Anat Embryol (Berl)* **211**, 367–377 (2006).

57. Chu, Y., Hughes, S. & Chan-Ling, T. Differentiation and migration of astrocyte precursor cells (APCs) and astrocytes in human fetal retina: relevance to optic nerve coloboma. *The FASEB Journal* **15**, 2013–2015 (2001).

58. Mellough, C. B. *et al.* An integrated transcriptional analysis of the developing human retina. *Development (Cambridge)* **146**, (2019).

59. Xue, Y. *et al.* CRALBP supports the mammalian retinal visual cycle and cone vision. *Journal of Clinical Investigation* **125**, 727–738 (2015).

60. Bernardos, R. L. & Raymond, P. A. GFAP transgenic zebrafish. *Gene Expression Patterns* **6**, 1007–1013 (2006).

61. Pende, M. *et al.* A versatile depigmentation, clearing, and labeling method for exploring nervous system diversity. *Sci Adv* **6**, eaba0365 (2020).

62. Kimura, T. *et al.* Guanine crystals regulated by chitin-based honeycomb frameworks for tunable structural colors of sapphirinid copepod, Sapphirina nigromaculata. *Sci Rep* **10**, (2020).

FIGURE LEGENDS

Figure 1. Mutation of GFAP is associated with retinal dysplasia and pseudopapilledema. **a.** Pedigree of a family with autosomal dominant retinal dysplasia, vision loss and pseudopapilledema. Affected individuals V.1, V.3, V.7, VI.4 and an obligate carrier IV.6 were heterozygous for a c.928dup variant (m) in *GFAP*, while three unaffected individuals (IV.4, V.8 and VI.3) were found not to be carriers (wt). **b.** Clinical data showing upper left panel: Fundus photographs of the optic disc of individuals V-1, V-3, V-7 and IV-6, right and left eye. Upper right panel: Macular- and optic nerve OCT of individuals V-1, V-3 and V-7. Lower panel: OCT of the optic nerve of individuals V-3, V-7 and IV-6. **c.** DNA sequence of *GFAP* nucleotide c.916-934 from a healthy (control) and an affected (c.928dup) individual.

Figure 2. GFAP is expressed in retinal neural progenitors. a-b. Sagittal section of human eye anlage at 35 dpc. **a.** Toluidine blue stained section. **a'.** Nestin (NES) immunostaining marks retinal neural progenitors (RNPs) in the NL. **b, b', b''.** Immunostaining shows strong expression of GFAP in RNPs within the NL. **c.** Sagittal section of human eye at 51 dpc. GFAP

immunostaining shows strong expression in early RNPs (black arrow), and weaker expression in more differentiated RNPs (grey arrows). **d-f.** Sagittal section of human eye at 13 wpc. Immunostaining show very weak GFAP expression (**d, e,** arrows) in Müller Glia Cells, marked by Vimentin (VIM) expression (**f**, arrows), but very strong GFAP expression in astrocytes, entering the retina from the optic nerve. LV: lens vesicle, LE: lens, NL: nervous layer, ON: optic nerve, PL: pigment layer, RE: retina, RPE: retinal pigment epithelium, VC: vitreous cavity.

Figure 3. The p.Met310Asnfs*113 variant protein have similar aggregate properties as WT GFAP *in vivo*. a. Quantification of GFAP aggregates in the brain and spinal cord of 30 hpf and 48 hpf larvae microinjected with 50 pg $GFAP^{WT}$, $GFAP^{Met310Asnfs*113}$ or $GFAP^{R79C}$ fusion construct. **a'.** High-magnification dorsal view ROI images of the head and trunk for each injected larvae group. Scale bar: 100 μm. **b.** Western blot analysis of the same microinjected larvae group as in (**a**); antibodies and protein size calculated as indicated. The data is presented as mean±sd. Asterisks indicate P-values obtained by using One-way ANOVA test: ****: $P < 0.0001$, ns: not significant.

Figure 4. Zebrafish promoter-less *gfap* mutants have smaller eyes which can be rescued with WT but not c.928dup mRNA. **a.** Dorsal view images of 2 and 6 dpf larvae head of WT and mutant siblings with or without injection of 100pg WT *gfap* mRNA or c.928dup mRNA. White bars indicate the major axis diameter for comparison. Measured mean eye diameter of both eyes for uninjected 2 dpf (**a'**) 6 dpf (**a''**) larvae and 6dpf larvae injected with WT (**b**) and c.928dup mRNA (**b'**). The data are presented as mean±sd. Asterisks indicate P-values obtained by using One-way ANOVA test: *: $P < 0.05$, **: $P < 0.01$, ****: $P < 0.0001$, ns: not significant. Scale bar: 50 μm.

Figure 5. Gross eye morphology is mildly affected in *gfap* promoter-less mutants. a. Hematoxylin and eosin staining of WT and mutant siblings eyes at different stages: 2, 4 and 6 dpf, scalebar, 50 μm, and 7 month old, scale bar, 500 μm. Higher magnification of retinal layers in 7 mpf fish. GCL, ganglion cell layer; IPL, inner plexiform layer; INL, inner nuclear layer; OPL, outer plexiform layer; ONL, outer nuclear layer; OS, outer segments; RPE, retinal pigment epithelium, scale bar, 50 μm. (**a**, bottom). **b.** Quantification of cells in the ganglion

cell layer from 6 dpf WT and mutant sibling eyes. **c.** Mean layer thickness in 7 mpf eyes. **d.** TUNEL assay of 36 hpf and 52 hpf eyes in the same group of WT and *gfap* mutant siblings, scale bar, 100 μm. **d'**. Quantification of apoptotic events in the eye of the same group as in (**d**). Asterisks indicate P-values obtained by using One-way ANOVA test: *: $P < 0.05$, **: $P < 0.01$, ***: $P < 0.001$, ns: not significant.

Figure 6. *gfap* promoter-less mutants are visually impaired. a. Startle-response assay. Experimental design (top). Diagram of the Zebrabox protocol showing at least 1 hour light adaptation phase and 3 minutes and 7 seconds testing phase consisting of seven dark periods and six light each with a duration of 1 second and 30 second, respectively. Plot of the mean distance travelled by 7 dpf WT and mutant siblings over the testing phase (bottom). **a'** (left) Distribution of larvae that respond to each Dark to light cycle (green) and not responding (red). **a'** (right) ANOVA analysis of mean responsive larvae among all the cycles. **b.** Representative locomotion of five 9 dpf larvae color-coded for swim speed (slow: black, intermediate: green, fast: red) for WT and mutant siblings. **b'** Bar plot of the duration spend at different swim speed: no activity, slow (<3mm/s), intermediate (3-8 mm/s) and fast (>8mm/s). Data is presented as mean±sd. Asterisks indicate P-values obtained by using One-way ANOVA test: *: $P < 0.05$, ***: $P < 0.001$, ****: $P < 0.0001$, ns: not significant.

Figure 7. MGCs, rods and double cones are abnormal in *gfap* promoter-less mutants. a. IFM analysis of $BLBP^+$ MGC in the INL of 4 dpf, 6 dpf and 7 mpf WT and mutant retina. Scalebar, 50 μm. Higher magnification of MGCs in ROI (white boxes). Blue arrowheads indicate weak BLBP expression in MGC apical processes at photoreceptor bases. White arrowheads indicate weak BLBP expression in MGC soma and distal processes. Scalebar, 20 μm. Green arrowheads indicate tearing with no DAPI staining in adult retina. **a'**. MGC count and cell body area in 4 and 6 dpf retinas from the same group of fish. **b.** IFM analysis of $ZPR3^+$ rods and double cones in the ONL 4 dpf, 6 dpf and 7 mpf WT and mutant retina. (b') Quantification of Rod/cone cell count of 4 and 6 dpf fish retina and photoreceptor volume in the same fish as well as in 7 mpf adult fish retina. **c.** 3D reconstruction of juvenile (14 dpf) and adult (9 mpf) eyes stained for $ZPR3^+$ rods and double cones. White circle highlights the pituitary macular region of the eye. Data is presented as mean±sd. Asterisks indicate P-values

obtained by using One-way ANOVA test: *: $P < 0.05$, **: $P < 0.01$, ***: $P < 0.001$, ****: $P < 0.0001$, ns: not significant.

Table 1. Clinical and genetic data on family

Position in pedigree	**IV-6**	**V-1**	**V-3**	**V-7**
Genotype GFAP	c.[928dup];[=]	c.[928dup];[=]	c.[928dup];[=]	c.[928dup];[=]
BCVA	Reported normal visus	RE: 1,25 (+0,75 -2,0 x 80º) LE: 1,25 (+0,75 -1,75 x 150º)	RE: 0,3 (+3,5 -2,25 x 80º) LE: 0,25 (+4,5 -1,0 x 145º) 2003: RE: 0,4 (+2,75 -2,25 x 70º) LE: 0,3 (+3,25 -1,0 x 90º)	RE:0,25 (+0,75) LE: 0,16 (-1,0 -2,0 x 0º) 2005: RE: 0,16 (+1,5 -2,25 x 170º) LE: 0,16 (+2,0 -2,75 x 5º)
Fundoscopic	Normal looking optic nerve head, retina, and vascular system	Pre- and peripapillary pellucid veil, normal optic nerve head, macular region and normal vessels	Massive pre-and peripapillary glial mass with sheeting of arterioles extending along the arcades. Distinct macular RPE atrophy in both macular regions	Pellucid pre- and peripapillary glial mass, massive central and peripheral vascular sheeting with a few splint hemorrhages. Diffuse RPE atrophy in the macular regions with pigment clumping.
Goldmann perimetry	Normal	Normal	Central scotoma both eyes	Central scotoma both eyes
Colour vision	NA	NA	Normal	Normal
Fullfield ERG	NA	NA	Normal	Normal
OCT	Normal optic nerve head, retina, and vascular system	Pre- and peripapillary pellucid optic veil where the inner retinal nerve layers melt together. Normal macular region	Confluent tissue mass of the inner retina around and in the optic nerve. The different retinal layers are “melted together” and cannot be differentiated. Sheeting of arterioles extending along the arcades. Macular atrophy in both macular regions. .	Confluent tissue mass of the inner retina around and in the optic nerve. The different retinal layers cannot be differentiated. Sheeting of arterioles extending along the arcades. The confluent tissue mass continues over and in the macular region as well as in the fovea.
Fluorescein angiography	NA	NA	NA	Vascularized epipapillary glial mass
Systemic signs	None	None	None	None

GFAP NC_000017.11, NM_002055.5 (GRCh38). WT: normal sequence in GFAP position c.928. BCVA: best corrected visual acuity. NA: not applied. RE: right eye; LE: left eye.

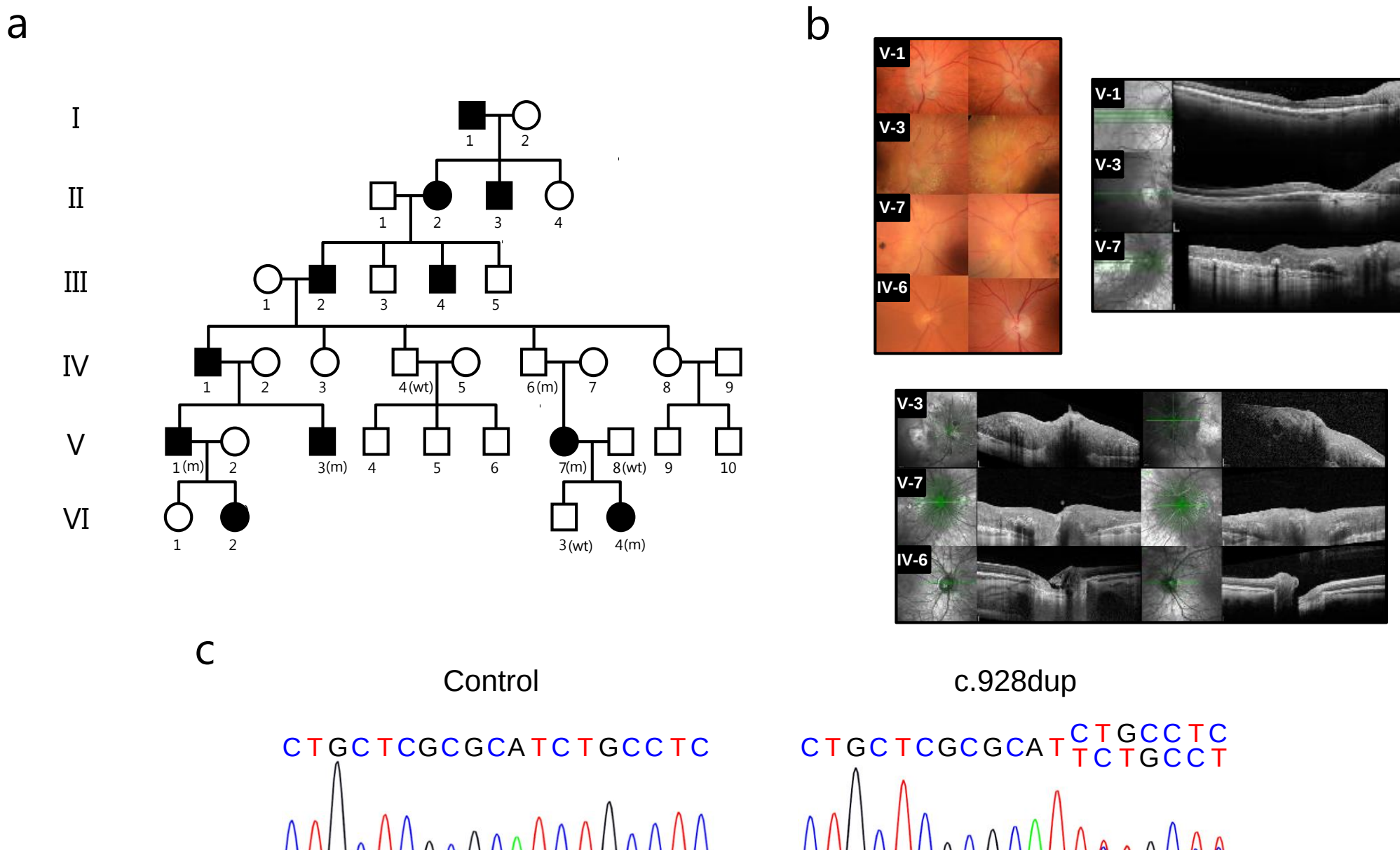
a
I
II
III
IV
V
VI
1
2
1
2
3
4
1
2
3
4
5
1
2
3
4(wt)
5
6(m)
7
8
9
1(m)
2
3(m)
4
5
6
7(m)
8(wt)
9
10
1
2
3(wt)
4(m)
b
V-1
V-3
V-7
IV-6
V-1
V-3
V-7
V-3
V-7
IV-6
c
Control
c.928dup
CTGCTCGCGCATCTGCCTC
CTGCTCGCGCAT CTGCCTC
TCTGCCT

FIGURE 1

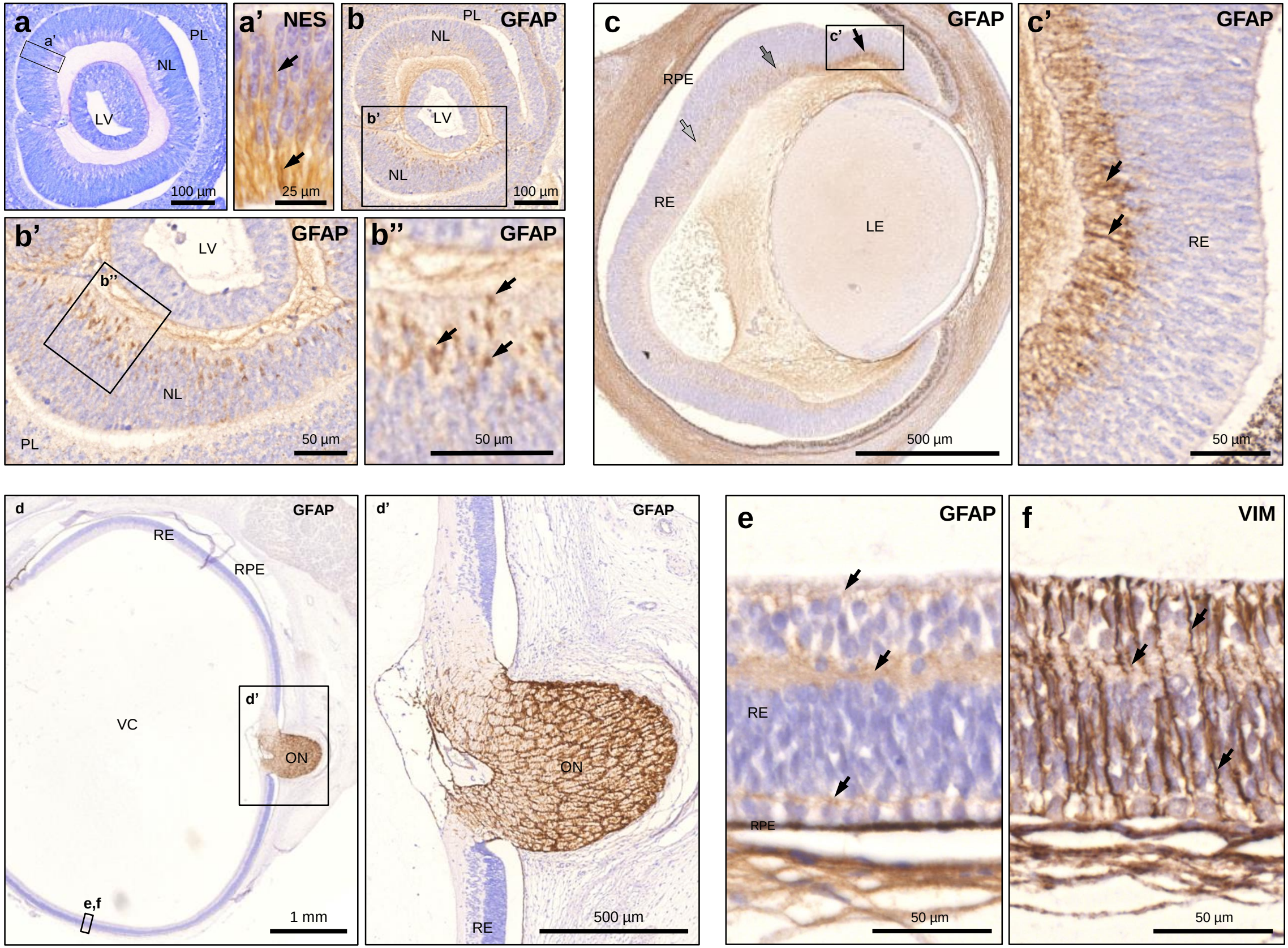
a
a'
PL
NL
LV
100 µm
a' NES
25 µm
b
PL
GFAP
NL
b'
LV
NL
100 µm
b'
GFAP
LV
b''
NL
PL
50 µm
b''
GFAP
50 µm
c
GFAP
c'
RPE
RE
LE
500 µm
c'
GFAP
RE
50 µm
d
GFAP
RE
RPE
VC
d'
ON
e,f
1 mm
d'
GFAP
ON
RE
500 µm
e
GFAP
RE
RPE
50 µm
f
VIM
50 µm

FIGURE 2

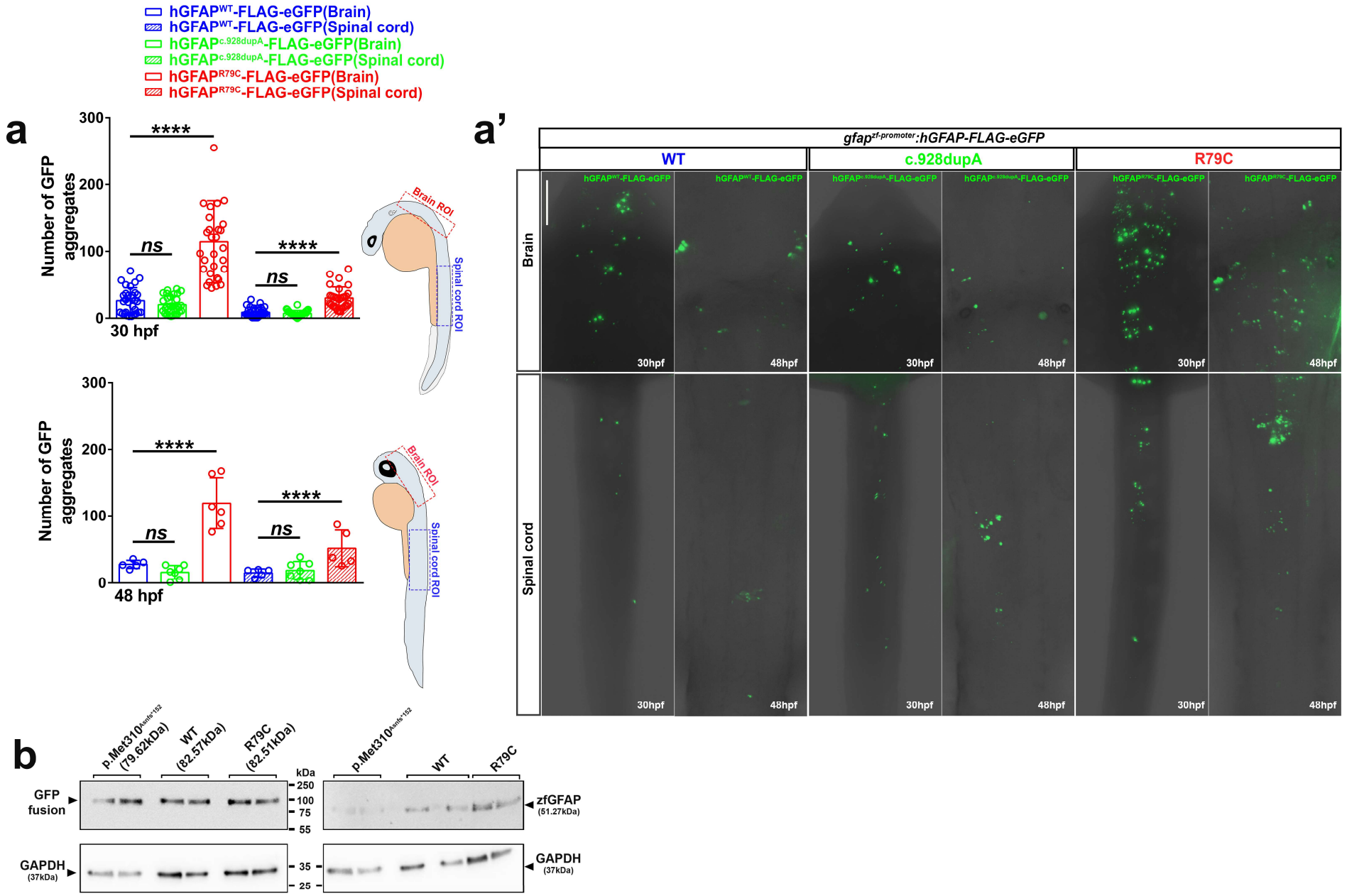
hGFAP^WT-FLAG-eGFP(Brain)
hGFAP^WT-FLAG-eGFP(Spinal cord)
hGFAP^c.928dupA-FLAG-eGFP(Brain)
hGFAP^c.928dupA-FLAG-eGFP(Spinal cord)
hGFAP^R79C-FLAG-eGFP(Brain)
hGFAP^R79C-FLAG-eGFP(Spinal cord)
a
Number of GFP aggregates
300
200
100
0
****
ns
****
ns
30 hpf
Brain ROI
Spinal cord ROI
48 hpf
a'
gfap^zf-promoter:hGFAP-FLAG-eGFP
WT
c.928dupA
R79C
Brain
Spinal cord
30hpf
48hpf
b
p.Met310^Δarnfs*152 (79.62kDa)
WT (82.57kDa)
R79C (82.51kDa)
kDa
250
100
75
55
35
25
GFP fusion
zfGFAP (51.27kDa)
GAPDH (37kDa)

FIGURE 3

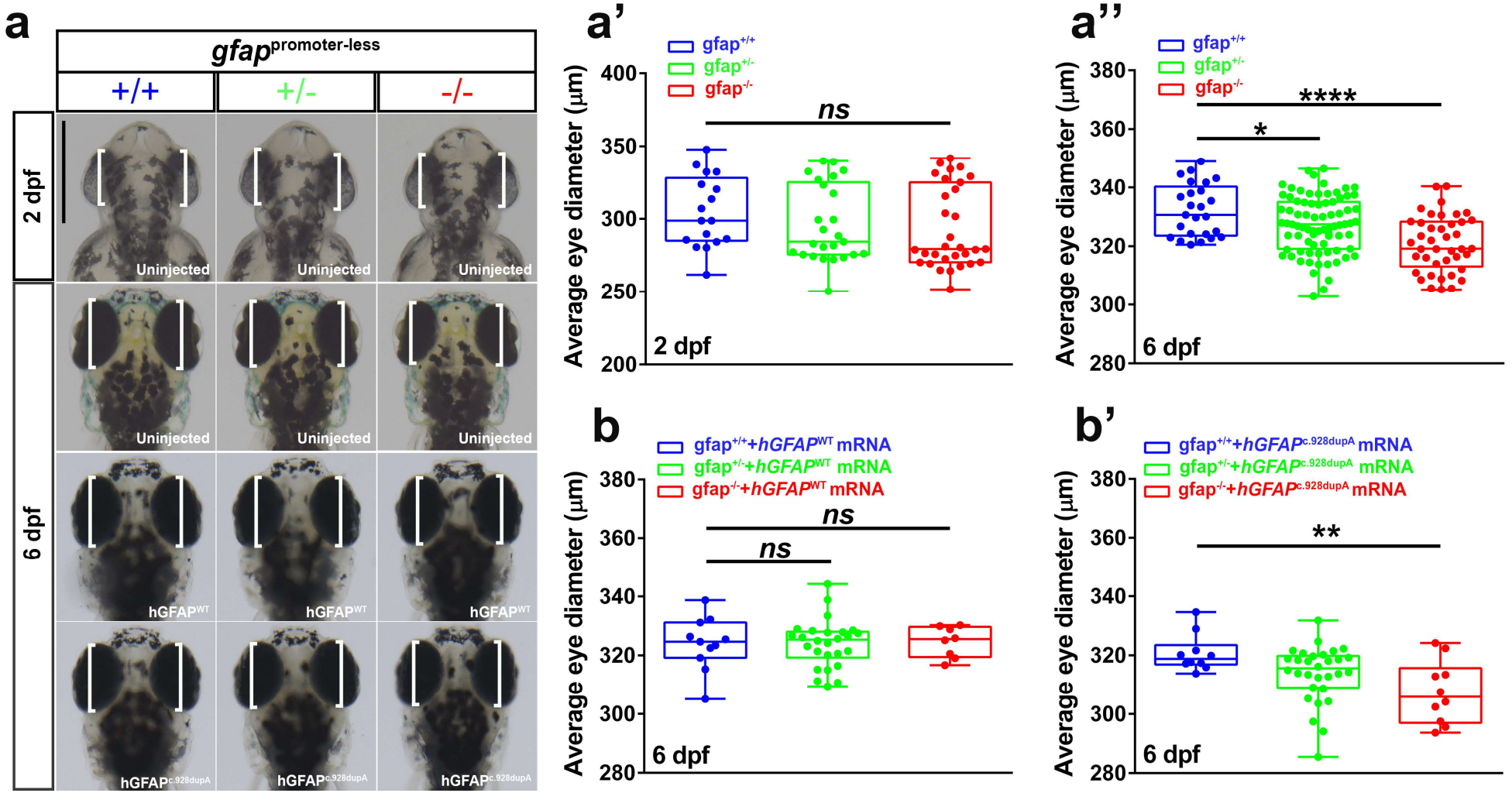
a
gfap promoter-less
+/+
+/-
-/-
2 dpf
6 dpf
Uninjected
hGFAP WT
hGFAP c.928dupA
a'
gfap +/+
gfap +/-
gfap -/-
ns
Average eye diameter (µm)
2 dpf
a''
****
*
6 dpf
b
gfap +/+ +hGFAP WT mRNA
gfap +/- +hGFAP WT mRNA
gfap -/- +hGFAP WT mRNA
ns
ns
b'
gfap +/+ +hGFAP c.928dupA mRNA
gfap +/- +hGFAP c.928dupA mRNA
gfap -/- +hGFAP c.928dupA mRNA
**

FIGURE 4

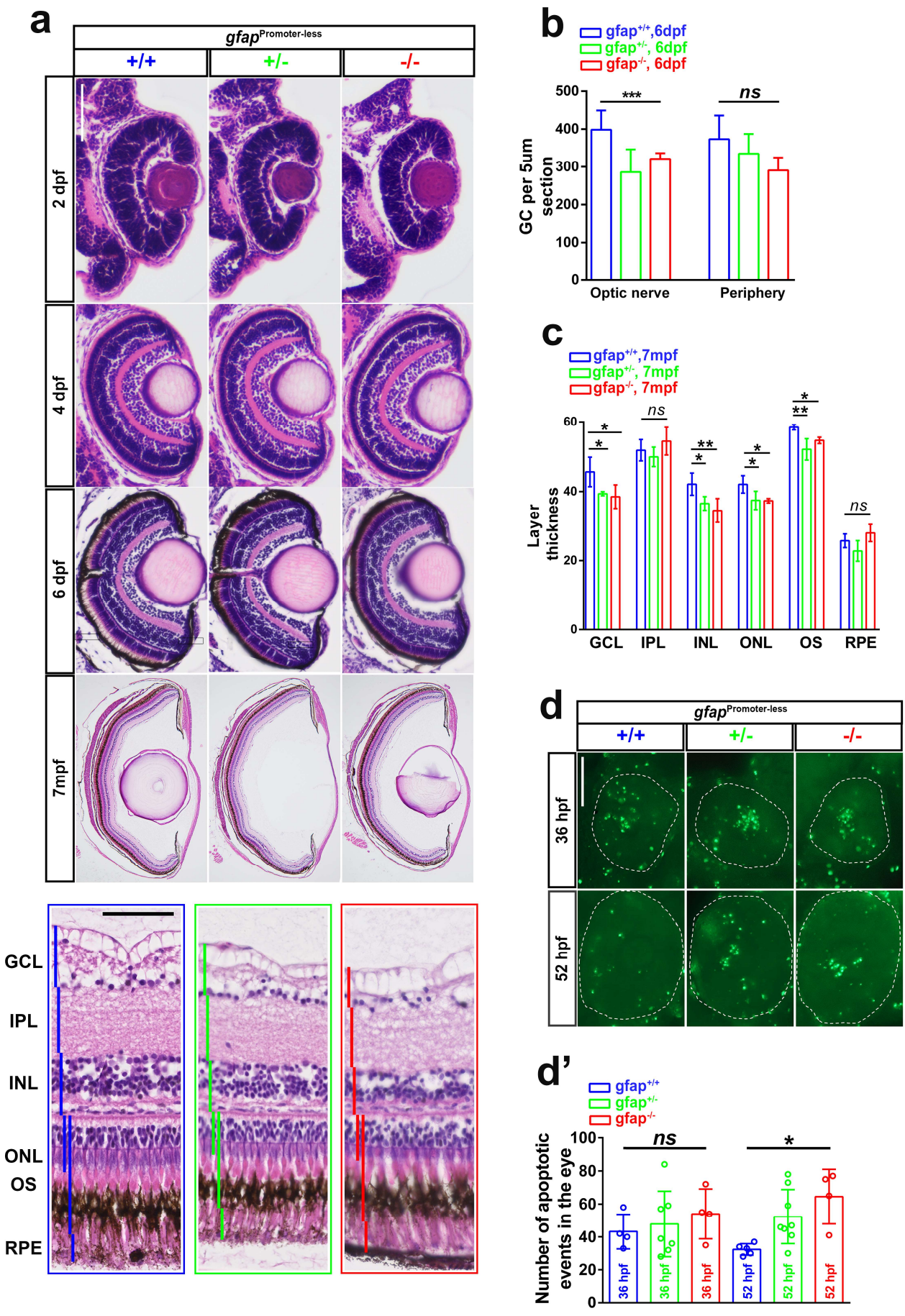
a
gfapPromoter-less
+/+
+/-
-/-
2 dpf
4 dpf
6 dpf
7mpf
GCL
IPL
INL
ONL
OS
RPE
b
gfap+/+,6dpf
gfap+/-, 6dpf
gfap-/-, 6dpf
GC per 5um section
500
400
300
200
100
0
***
ns
Optic nerve
Periphery
c
gfap+/+,7mpf
gfap+/-, 7mpf
gfap-/-, 7mpf
Layer thickness
60
40
20
0
*
*
ns
**
*
*
*
**
ns
GCL
IPL
INL
ONL
OS
RPE
d
gfapPromoter-less
+/+
+/-
-/-
36 hpf
52 hpf
d'
gfap+/+
gfap+/-
gfap-/-
Number of apoptotic events in the eye
100
80
60
40
20
0
ns
*
36 hpf
36 hpf
36 hpf
52 hpf
52 hpf
52 hpf

FIGURE 5

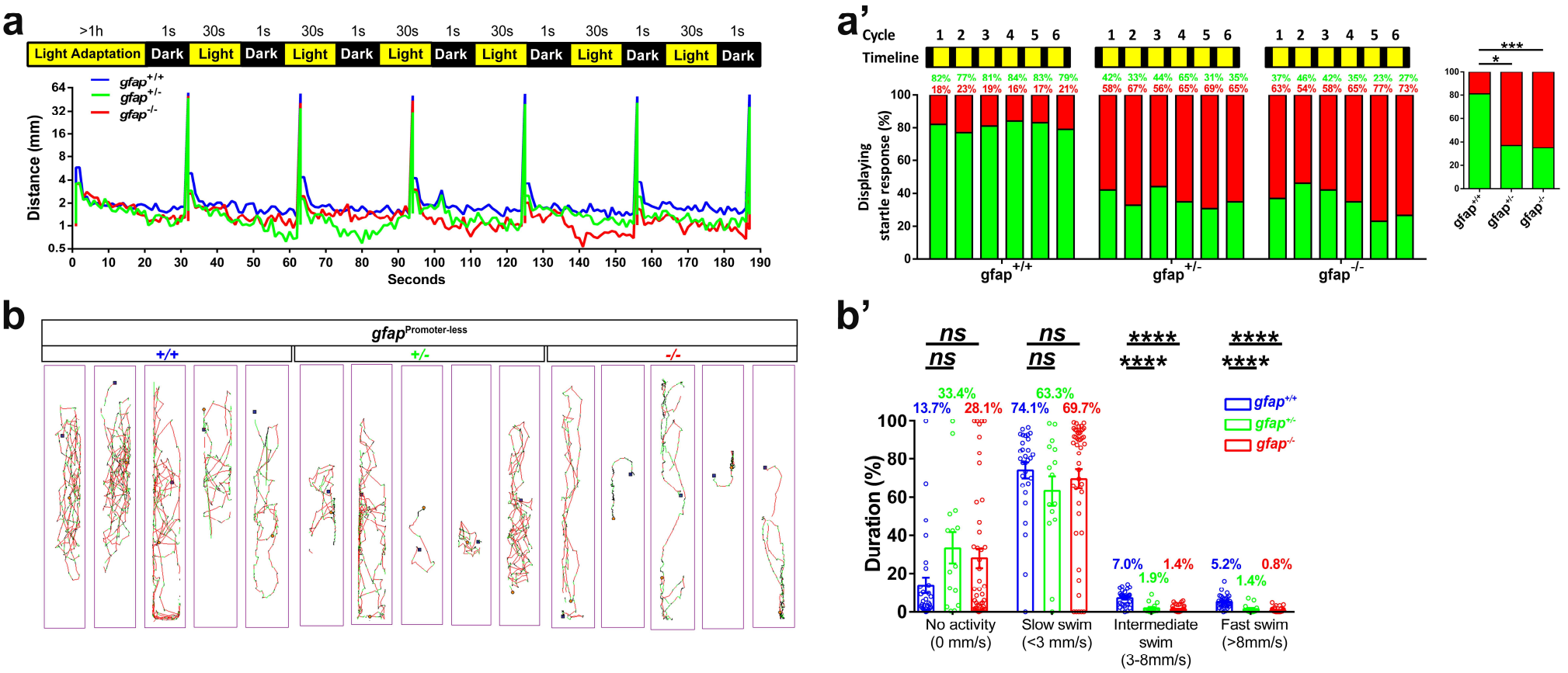
a
>1h
1s
30s
Light Adaptation
Dark
Light
gfap+/+
gfap+/-
gfap-/-
Distance (mm)
Seconds
a'
Cycle
Timeline
Displaying startle response (%)
gfap+/+
gfap+/-
gfap-/-
b
gfapPromoter-less
+/+
+/-
-/-
b'
ns
****
Duration (%)
No activity (0 mm/s)
Slow swim (<3 mm/s)
Intermediate swim (3-8mm/s)
Fast swim (>8mm/s)

FIGURE 6

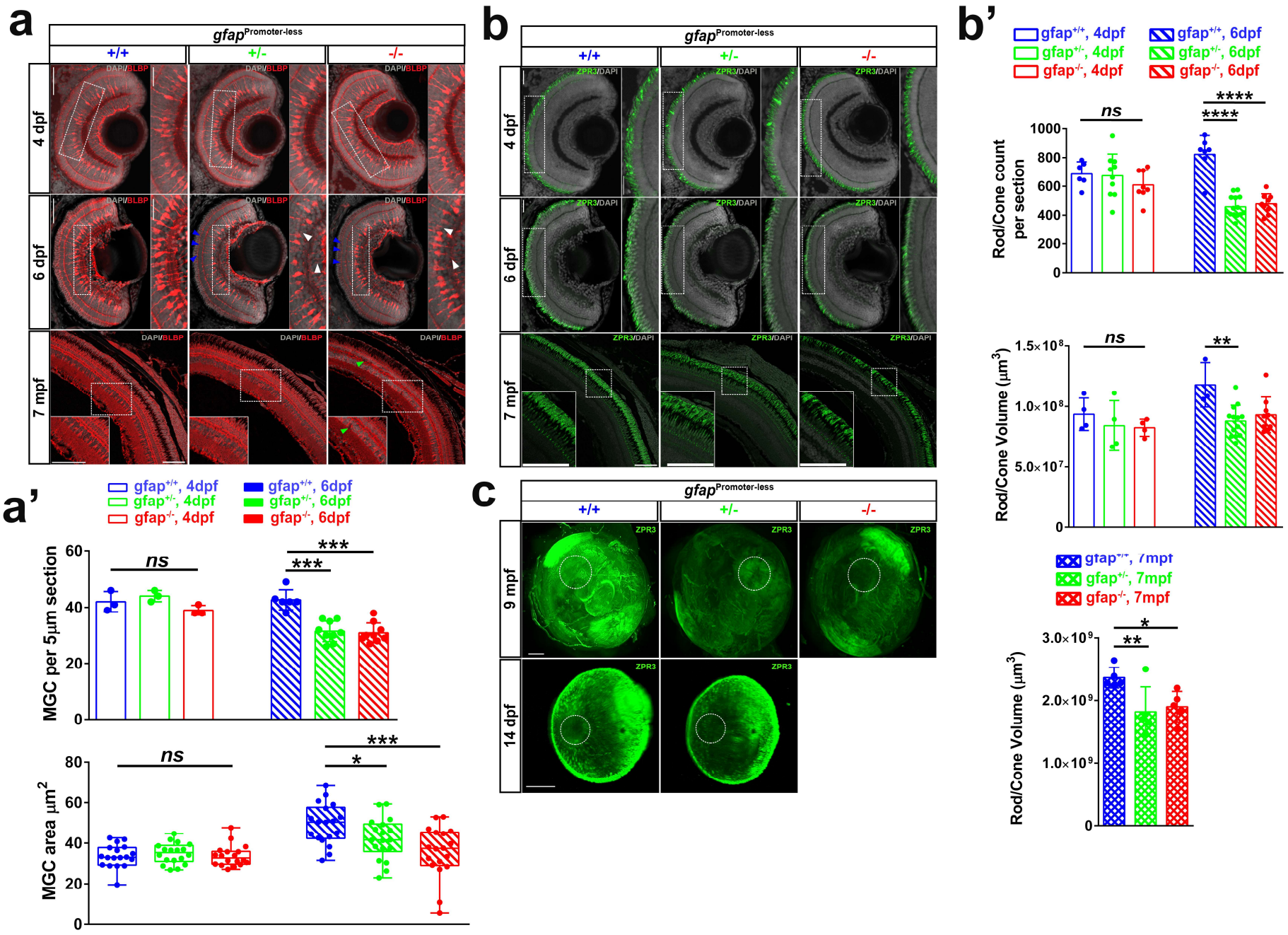
a
gfapPromoter-less
+/+
+/-
-/-
4 dpf
6 dpf
7 mpf
DAPI/BLBP
b
ZPR3/DAPI
9 mpf
14 dpf
ZPR3
c
a'
gfap+/+, 4dpf
gfap+/-, 4dpf
gfap-/-, 4dpf
gfap+/+, 6dpf
gfap+/-, 6dpf
gfap-/-, 6dpf
MGC per 5µm section
MGC area µm2
ns
***
*
b'
Rod/Cone count per section
Rod/Cone Volume (µm3)
gfap+/+, 7mpf
gfap+/-, 7mpf
gfap-/-, 7mpf
****
**

FIGURE 7